Taylor & Francis
Taylor & Francis Group

Numerical Heat Transfer, Part A: Applications
An International Journal of Computation and Methodology

ISSN: (Print) (Online) Journal homepage: https://www.tandfonline.com/loi/unht20

Theoretical modeling and verification of storage time of cold box based on network method of radiation heat transfer

Zhiqiang Fu, Haozhe Liu, Liying Duan, Liqiang Huang & Yan Wang

To cite this article: Zhiqiang Fu, Haozhe Liu, Liying Duan, Liqiang Huang & Yan Wang (2024) Theoretical modeling and verification of storage time of cold box based on network method of radiation heat transfer, Numerical Heat Transfer, Part A: Applications, 85:2, 203-221, DOI: 10.1080/10407782.2023.2181244

To link to this article: https://doi.org/10.1080/10407782.2023.2181244


Published online: 23 Mar 2023.


Submit your article to this journal


Article views: 49


View related articles


View Crossmark data

Full Terms & Conditions of access and use can be found at
https://www.tandfonline.com/action/journalInformation?journalCode=unht20

NUMERICAL HEAT TRANSFER, PART A: APPLICATIONS
2024, VOL. 85, NO. 2, 203–221
https://doi.org/10.1080/10407782.2023.2181244

Taylor & Francis
Taylor & Francis Group

Check for updates

Theoretical modeling and verification of storage time of cold box based on network method of radiation heat transfer

Zhiqiang Fu[a], Haozhe Liu[a], Liying Duan[b], Liqiang Huang[a], and Yan Wang[c]

[a]School of Light Industry Science and Engineering, Tianjin University of Science and Technology, Tianjin, P.R. China; [b]Department of Transportation and Vehicle Engineering, Tangshan College, Hebei, P.R. China; [c]College of Mechanical Engineering, Tianjin University of Science and Technology, Tianjin, P.R. China

ABSTRACT

The storage time of cold box is an important subject. At present, the research method of the storage time is mainly an experiment, and the theoretical research is incomplete. Therefore, in this work, theoretical modeling combined with a network method of radiation heat transfer, the shape factor of heat conduction, and sensible heat of refrigerant were proposed to calculate the storage time of a cold box at various ambient temperatures and amounts of refrigerant. The experimental and simulation results were used to verify the theoretical modeling of the storage time. The influences of the sensible heat of refrigerant and radiation heat transfer in the cold box were analyzed. The stability of the theoretical modeling was studied via simulation of the different cold box and refrigerant materials. The results of the accuracy of the theoretical model confirmed that the maximum error between the theoretical and the experimental storage times is 8.45%, and the error between the theoretical and the simulation results is 7.51%, indicating that the sensible heat of refrigerant and radiation heat transfer have big impacts on the storage time. The stability of the theoretical model is confirmed under the different box and refrigerant materials, and different shapes of refrigerant. The storage time model has stability on different box materials and refrigerant materials. The theoretical model can be severed as a fundamentally guidance for the cold box production design.

ARTICLE HISTORY
Received 13 October 2022
Revised 6 February 2023
Accepted 9 February 2023

KEYWORDS
Cold box; Fluent; network method of radiation heat transfer; shape factor; storage time

1. Introduction

The cold box can ensure the integrity of cold chain transportation; thus, it plays an important role in cold chain transportation [1]. The ratio of the change of thermal energy and mechanical energy in the refrigerant to the heat flow during heat transfer is denoted as the storage time of the refrigerant based on the principle of energy conservation [2].

The change of thermal energy and mechanical energy in the cold box is mainly determined by the heat absorption of the refrigerant. The material used for the refrigerant is mainly phase change material. The phase change material has two ways to absorb heat: sensible heat and latent heat [3]. Sensible heat is a response of the refrigerant to the environmental change due to the increase in ambient temperature, which mainly occurs in the solid or liquid phase of the refrigerant [4]. Latent heat is due to the morphological transformation of the refrigerant and the absorption of the heat from the surrounding environment, which occurs in the phase change stage of

CONTACT Zhiqiang Fu fzq6670300@163.com School of Light Industry Science and Engineering, Tianjin University of Science and Technology, Tianjin 300457, P.R. China.

© 2023 Taylor & Francis Group, LLC

Nomenclature

A_i, A_j A_k	the surface area of i, m^2; j, m^2; and k, m^2	l	inner side length, m
		L	distance between two planes, m
A_{wall}	inner surface area, m^2	M	mass of the refrigerant, kg
A_1	refrigerant area, m^2	s, s_{corner}, s_{edge}, s_{wall}	shape factor, m
A_2	top surface area of cold box, m^2	T_s	phase change temperature, °C
A_3	flank area of cold box, m^2	T_{sur}	ambient temperature, °C
B, Z	the width of the i and j surface	T_0	initial temperature of refrigerant, °C
c	specific heat of refrigerant, $Jkg^{-1}{}^{\circ}C^{-1}$	x	wall thickness, m
C	common edge length of two planes, m	X, Y	the length, m and the width, m of i surface
E_g	additional thermal energy, J	$X_{i,j}$	perspective coefficient
E_{in}	energy of the outside world entering the cold box, J	ε_1, ε_2	emissivity
		σ	Stefan–Boltzmann constant
E_{out}	energy from the cold box to the outside world, J	ΔE_{st}	change of thermal energy and mechanical energy in the cold box, J
h_{sf}	latent heat, $J.kg^{-1}$		
k	thermal conductivity of cold box, $Wm^{-1}{}^{\circ}C^{-1}$	Δt, Δt_0	storage time, s
		Φ	heat flow of heat conduction, W

the refrigerant [5]. Bai *et al.* [6] and Jia *et al.* [7] used latent heat of phase change when calculating the storage time. There is no research on the storage time of cold box considering the sensible heat of refrigerant. Therefore, in this work, the theoretical models established with and without solid sensible heat are compared with the experimental results to analyze the influence of solid sensible heat of refrigerant on the storage time.

Heat transfer takes place through conduction, convection, and radiation. Song *et al.* [5] and Ryms and Lewandowski [8] ignored the convective heat transfer in the cold box when the refrigerant was placed at the bottom because the air flow inside the box was not apparent. In this article, different fluid flow models are used to simulate the temperature field distribution of the incubator to analyze whether the convective heat transfer can be neglected. The conduction in the cold box is mainly caused by the varying temperature distribution on both sides of the box. Du *et al.* [9] and Zhao *et al.* [10] studied the effective heat transfer area in the calculation of conduction heat transfer. Wang *et al.* [11] used the shape factor to divide the 3D model of a cold box into various 2D heat transfer for calculation. The conduction heat transfer in the cold box plays a dominant role [3, 5, 12]. Tan *et al.* [13] and Xiaofeng and Xuelai [14] only used conduction heat transfer in the calculation and ignored radiation heat transfer to simplify the computation of storage time. However, Sharma *et al.* [15] and Paquette *et al.* [16] found that the radiation heat transfer in the cold box has a remarkable effect on the temperature in the box by adding aluminum foil to the inner wall of the cold box, when the temperature difference between inside and outside cold box is large. Thus, the effect of radiation heat transfer on thermal insulation performance is studied in this work.

The theoretical research on the radiation of the cold box is mainly regarded as the blackbody radiation inside the cold box [16]. However, radiation heat transfer is greatly related to the distance between the planes [17, 18]. The approximate blackbody radiation calculation equation has certain limitations. The blackbody radiation calculation equation did not consider the calculation of radiation heat transfer at different positions. Therefore, in this work, the cold box is divided according to the temperature boundary by the current and the voltage in the analogy circuit, and the visual coefficient related to the distance between the two planes is introduced to establish the radiation heat transfer grid. According to Kirchhoff's current law [19], the total current flowing

into each node and the total radiation heat flux of each node in the radiation heat transfer network method are zero.

In the simulation of the cold box, the temperature distribution and storage time can be simulated by software, which can greatly reduce time, manpower, and material resources. Selecting the computational fluid dynamics (CFD) model in the cold box is necessary. Ambaw *et al.* [20] and Zhang *et al.* [21] found that the cold box was more suitable for the laminar flow model, according to the different CFD models summarized. The selection of a radiation model is a main concern in the numerical simulation of radiation heat transfer [22, 23]. The discrete ordinate (DO) radiation model in Fluent software covers the entire optical thickness and can solve the surface-to-surface (S2S) radiation [24]. Zhao *et al.* [22] and Yu *et al.* [25] found that adding a DO radiation mode in Fluent could more accurately simulate the thermal insulation performance of the cold box. However, Wu and Zhang [26] used the S2S radiation model to analyze the thermal insulation performance of the cold box. There is seldom reported on the influence of different radiation models on the storage time and temperature distribution of the cold box. In this work, the influence of adding S2S radiation model or DO radiation model on the storage time and temperature distribution of cold box is analyzed.

In this research, the theoretical modeling of storage time with radiation heat transfer is established, and the influences of radiation heat transfer and sensible heat on the cold box are analyzed. The shape factor, sensible heat, and the network method of radiation heat transfer are introduced to establish the storage time of the cold box. The accuracy of storage time theoretical modeling is verified by comparing the experimental and numerical results. The stability of theoretical modeling is verified by simulation modeling using different cold box and refrigerant materials, which provides a theoretical basis for the future.

2. Methods

2.1. Theoretical model of storage time

The cold box is composed of a box body and refrigerant. The storage time of the cold box refers to the time from putting the refrigerant into the cold box to the end of the phase change of the refrigerant [25]. The refrigerant in the cold box is described from an energy balance as follows [19]:

$$\Delta E_{st} = E_{\text{in}} - E_{\text{out}} + E_g \tag{1}$$

where ΔE_{st} is the change of thermal energy and mechanical energy in the refrigerant during the storage time, E_{in} is the energy of the outside world entering the refrigerant, E_{out} is the energy from the refrigerant to the outside world, and E_g is the additional thermal energy like biological respiratory heat, combustion heat, and electric heat [19].

ΔE_{st} is composed of latent heat of the phase change of the refrigerant and sensible heat from the initial temperature to phase change temperature [6]:

$$\Delta E_{st} = Mh_{sf} + cM(T_s - T_0) \tag{2}$$

where M is the mass of the refrigerant; h_{sf} is the melting latent heat, that is, the energy required for the transformation of the solid to liquid per mass; c is the specific heat capacity, T_s is the phase transition temperature, and T_0 is the initial temperature.

As for refrigerant, the energy of the outside world entering the refrigerant includes heat transfer conduction and heat transfer convection, and the convective heat transfer in the cold storage cold box is ignored; as shown in Eq. (3) [27]:

$$E_{\text{in}} = ks(T_{\text{sur}} - T_s)\Delta t \tag{3}$$

where Δt is the time, where k is the thermal conductivity, T_{sur} is the ambient temperature, T_s is

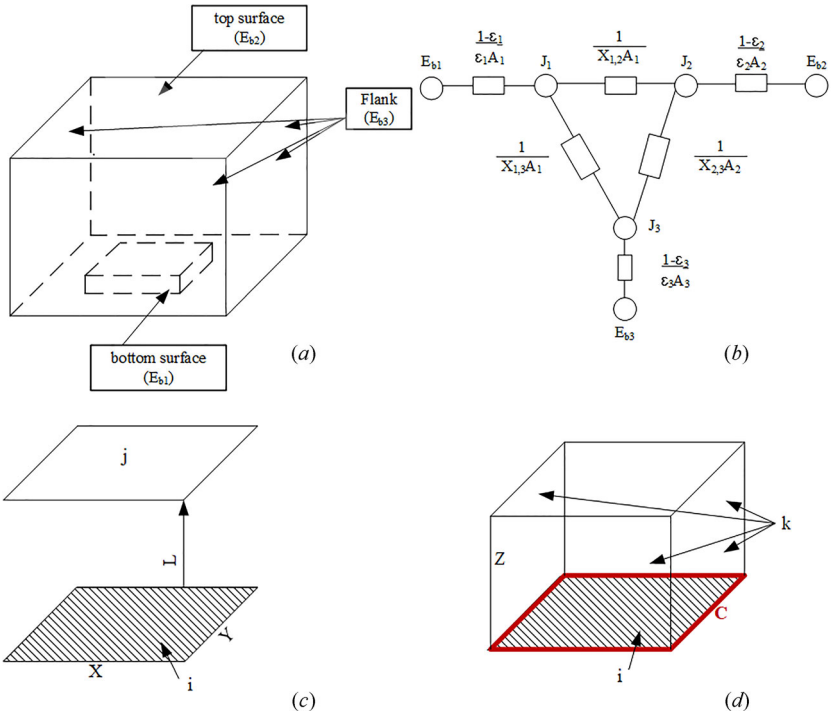

Figure 1. Calculation method of radiant heat transfer grid for the cold box: (*a*) temperature boundary division of the cold box, (*b*) equivalent network diagram of three-surface closed cavity, (*c*) parameters of two parallel rectangles, and (*d*) parameters of the mutually perpendicular rectangle with common edges.

the phase change temperature of the refrigerant, and s is the shape factor. The expression of s in the cold box is as follows [11]:

$$s = s_{\text{corner}} + s_{\text{edge}} + s_{\text{wall}} \tag{4}$$

$$s_{\text{corner}} = \sum 0.15L \tag{4a}$$

$$s_{\text{edge}} = \sum 0.54l \tag{4b}$$

$$s_{\text{wall}} = \sum \frac{A_{\text{wall}}}{L} = \frac{\sum A_{\text{wall}}}{L} \tag{4c}$$

where L is the wall thickness, l is the inner side length of the cold storage incubator, and A_{wall} is the inner surface area.

As for refrigerant, the energy released from the inside of refrigerant to the outside includes radiation heat transfer and heat transfer convection, and the convective heat transfer in the cold storage cold box is ignored as shown in Eq. (5) [27]:

$$E_{\text{out}} = E_{\text{rad}} \tag{5}$$

In the calculation of radiation, the surface-to-surface radiation is used to establish the theoretical model. The whole cold box is divided into three surfaces according to temperature boundary, namely, bottom, top, and side. Calculation is carried out by the network method of radiation heat transfer, as shown in Figure 1 [19]:

Three surfaces form a closed cavity. The radiant heat flow at each node is 0 by analogy with Kirchhoff's current law, allowing three equations to be constructed:

$$\begin{cases} \dfrac{E_{b1}-J_1}{\frac{1-\varepsilon_1}{\varepsilon_1 \ A_1}}+\dfrac{J_2-J_1}{\frac{1}{X_{1,2} \ A_1}}+\dfrac{J_3-J_1}{\frac{1}{X_{1,3} \ A_1}}=0 \\ \dfrac{J_1-J_2}{\frac{1}{X_{2,1} \ A_2}}+\dfrac{E_{b2}-J_2}{\frac{1-\varepsilon_2}{\varepsilon_2 \ A_2}}+\dfrac{J_3-J_1}{\frac{1}{X_{2,3} \ A_2}}=0 \\ \dfrac{J_1-J_3}{\frac{1}{X_{3,1} \ A_3}}+\dfrac{J_2-J_3}{\frac{1}{X_{3,2} \ A_3}}+\dfrac{E_{b3}-J_3}{\frac{1-\varepsilon_2}{\varepsilon_2 \ A_3}}=0 \end{cases} \tag{6}$$

In Eq. (6): J_i is effective radiation, ε_1 is the emissivity of ice, ε_2 is the emissivity of XPS, $E_{b1}=T_s^4\sigma$, $E_{b2}=E_{b3}=T_{sur}^4\sigma$, and $\sigma=5.67\times10^{-8}\mathrm{Wm^{-2}K^{-4}}$; $\varepsilon_1=0.96,\varepsilon_2=0.90$.where $X_{i,\ j}$ is the perspective coefficient [19], which is the fraction of radiation from surface i intercepted by surface j. The visual coefficient of the two neatly arranged parallel rectangles is expressed as follows [19]:

$$X_{i,j}=\frac{2}{\pi\overline{X}\overline{Y}}\left\{\begin{array}{l} \ln\left[\dfrac{\left(1+\overline{X}^2\right)\left(1+\overline{Y}^2\right)}{\left(1+\overline{X}^2+\overline{Y}^2\right)}\right]^{1/2}+ \\ \overline{X}\left(1+\overline{Y}^2\right)^{1/2}\tan^{-1}\left(\dfrac{\overline{X}}{\left(1+\overline{Y}^2\right)^{1/2}}\right)+ \\ \overline{Y}\left(1+\overline{X}^2\right)^{1/2}\tan^{-1}\left(\dfrac{\overline{Y}}{\left(1+\overline{X}^2\right)^{1/2}}\right)-\overline{X}\tan^{-1}\overline{X}-\overline{Y}\tan^{-1}\overline{Y} \end{array}\right\} \tag{7}$$

$$\overline{X}=\frac{X}{L},\quad \overline{Y}=\frac{Y}{L} \tag{7a}$$

where X and Y are the length and the width of i surface (bottom surface in Figure 1*a*), respectively; and L is the distance between two planes as shown in Figure 1*c*.

The visual coefficient of the mutually perpendicular rectangle with common edges is shown in Eq. (8) [19]:

$$X_{i,k}=\frac{1}{\pi W}\left(\begin{array}{l} W\tan^{-1}\dfrac{1}{W}+H\tan^{-1}\dfrac{1}{H}1- \\ \left(H^2+W^2\right)^{1/2}\tan^{-1}\left(\dfrac{1}{\left(H^2+W^2\right)^{1/2}}\right)+ \\ \dfrac{1}{4}\ln\left\{\dfrac{(1+W^2)(1+\mathrm{H}^2)}{1+W^2+H^2}\left[\dfrac{W^2(1+W^2+H^2)}{(1+W^2)(1+H^2)}\right]^{W^2}\times\right\} \\ \left[\frac{H^2(1+W^2+H^2)}{(1+W^2)(1+H^2)}\right]^{H^2} \end{array}\right) \tag{8}$$

$H=\ \frac{Z}{C},\ W=1$ (8*a*)where Z is the width of the k surface (flank surface in Figure 1*a*), C is the common edge length of i and k surfaces (perimeter of bottom surface in Figure 1*a*), as shown in Figure 1*d*. The visual coefficient relation has two important relations [19]: one is the interchange relation, such as Eq. (9), and the other is the summation relation, such as Eq. (10):

$$A_i\ X_{i,j}=A_j\ X_{j,i}=A_kX_{k,i} \tag{9}$$

where A_i is the surface area of i, A_j is the surface area of j, and A_k is the surface area of k.

$$\sum\nolimits_{j=1}^{N}X_{i,j}=1 \tag{10}$$

where N is the number of i radiating to each surface. If i is a single surface, then $X_{i,\ j}$=0.

The ratio of difference between E_{b1} and J_1 and $\frac{1-\varepsilon_1}{\varepsilon_1 A_1}$ is the radiation heat flow of refrigerant. The radiation of refrigerant is the multiplication of radiation heat flow and storage time [19], as shown in Eq. (11):

$$E_{\text{rad}} = \frac{|E_{b1} - J_1|}{\frac{1-\varepsilon_1}{\varepsilon_1 A}} \Delta t \tag{11}$$

Equation (1) has no heat generation for the refrigerant; thus, $E_g = 0$. The new storage time model is combined Eqs. (1)–(3) and (12) as follows:

$$\Delta t = \frac{M\Delta h_{sf} + cM(T_s - T_0)}{ks(T_{\text{sur}} - T_s) - \frac{|E_{b1} - J_1|}{\frac{1-\varepsilon_1}{\varepsilon_1 A}}} \tag{12}$$

The error is the summation relation such as Eqs. (13) and (14):

$$\text{error} = \frac{|\Delta t - \Delta t_{t0}|}{\Delta t_{t0}} \times 100\% \tag{13}$$

where Δt is the storage time of theoretical model; Δt_{t0} is the storage time of experiment.

$$\text{error} = \frac{|\Delta t - \Delta t_{t1}|}{\Delta t_{t1}} \times 100\% \tag{14}$$

where Δt_{t1} is the storage time of simulation.

2.2. Finite element simulation model description

2.2.1. Physical model

A physical model of the cold box is built using Creo 2.0. A 3D structure of the box, including a box at the outside, a refrigerant part at the bottom of the box, and an air part surrounding the refrigerant is illustrated in Figure 2. The internal dimension of the cold box is 350 mm ×

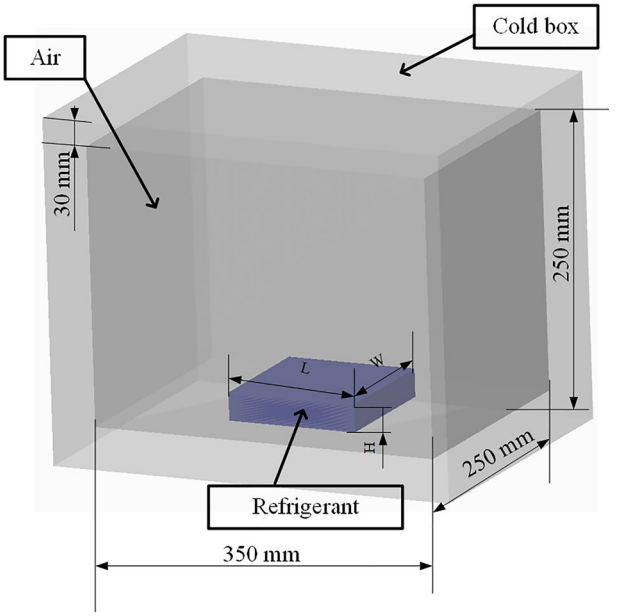

Figure 2. Schematic of the cold box model.

Table 1. Size of the refrigerant in different cases.

Refrigerant (piece)	Length (mm)	Width (mm)	Height (mm)
24	130	130	25
48	180	180	
72	220	220	
96	275	250	

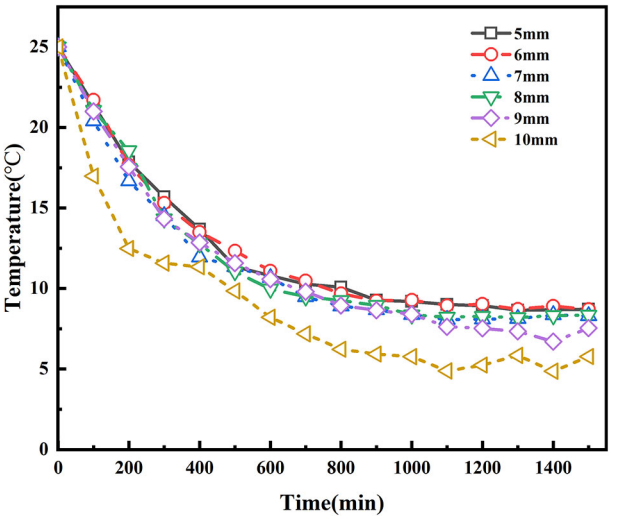

Figure 3. Verification of mesh independence.

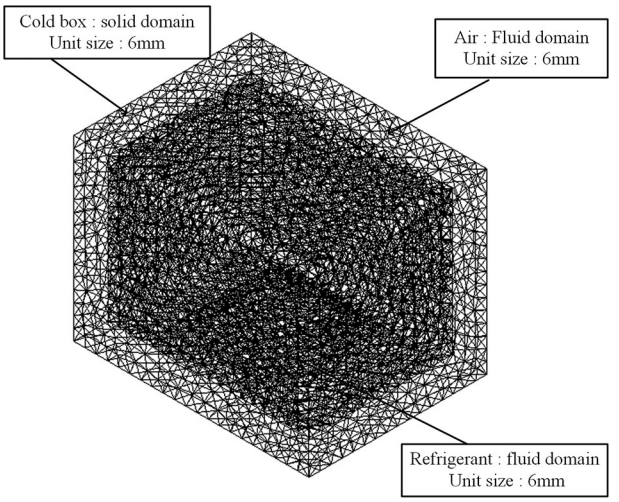

Figure 4. Meshing of cold box.

250 mm× 250 mm, and the wall thickness is 30 mm. The different sizes of refrigerant are shown in Table 1.

Mesh division is conducted using CFD ICEM. The air part in the cold box needs to be carefully separated when dividing the mesh. Mesh independence verification is necessary to reduce the computation cost and time. The midpoints in the cold box in the finite element simulation results of the different mesh sizes are extracted for the result analysis. The mesh independence result is shown in Figure 3. When the mesh size is reduced to 6 mm, the mesh size continues to shrink. At this time, the fluctuation of the finite element simulation results is small, and the small

Table 2. Material properties of each part of the box.

Materials	Thermal conductivity ($Wm^{-1}{}^{\circ}C^{-1}$)	Density (kgm^{-3})	Specific heat ($Jkg^{-1}{}^{\circ}C^{-1}$)
XPS	0.03	33	1500
Refrigerant	2.22	900	2100
Air	0.024	1.161	1006

Table 3. Calculation module settings.

Models	Details
Energy equation	Open energy equation, melting, and soilding
Viscous	Laminar
Radiation	S2S model and off solar load
Gravity	9.81 ms^{-2}
Boundary conditions	The no-slip boundary is used on all wall surfaces. The thermal conditions of the outer wall of the cold box are set to temperature, and the values are consistent with the ambient temperature of 25 °C, 35 °C, and 45 °C. The other boundary conditions are coupled.
Monitors	Temperature monitoring points are set in the middle of the cold box, the middle of the cold box and the middle of the top surface of the cold box, and the recording frequency is the length of each step
Time step size	60 s
Maximum number of iterations	20

nuances generated can be ignored. As shown in Figure 3, the mesh size of the air part is 6 mm after mesh independence verification.

To ensure the convergence of the simulation results, the mesh size of the two other parts is consistent with that of the air part. A hexahedral mesh is used. The mesh division results of the cold box are shown in Figure 4.

2.2.2. The settings of simulation model

The finite element model that describes the temperature inside the box is created. Each item inside the box is treated as a continuum. The model considers the complexity of the 3D heat transfer of the box. The main hypotheses underlying the model are as follows:

1. The cold box is considered to be completely sealed, and gaps between walls are ignored.
2. The calculation uses the Boussinesq hypothesis [28]. Each physical property is regarded as a constant and does not change during the process.
3. The volumetric change of refrigerant during a phase change is neglected.

2.2.3. Numerical realization

The whole mesh file of the cold box is imported into Fluent to unify the mesh units. The mesh quality is checked to observe whether it meets the calculation requirements, and the material properties of the different parts are shown in Table 2.

The numerical model is implemented using ANSYS Fluent19.2. The momentum equations and the volume fractions are spatially discretized using the second-order upwind method and the time term is discretized by implicit scheme. The pressure–velocity coupling equation is derived using the phase-coupled SIMPLEC algorithm. The solution method for the pressure is "standard." The details of other settings are shown in Table 3.

2.3. Experiments distribution

2.3.1. Experimental materials and equipment

The materials of cold box, air, and refrigerant are the same as Table 2. The influence of temperature on the thermal conductivity of XPS is not significant [29]. The size of the cold box is

Table 4. The information and use of equipment.

Equipment	Serial number	Manufactures	Use
Multichannel temperature tester	AT4508-128	Changzhou Anbai Precision Instrument, China	Record the temperature change inside the cold box in real time.
Constant temperature and humidity chamber	ETH-408-40-CP-AR	Jufu Instrument, China	Simulate the environmental temperature and humidity during transport
Refrigerator	MDF-339-C	Dalian Sanyang Cold Chain, China	Freeze the refrigerant
Sawing machine	BSM-400	Tianjin Zhihua Mechanical Electronics, China	Cut XPS plates

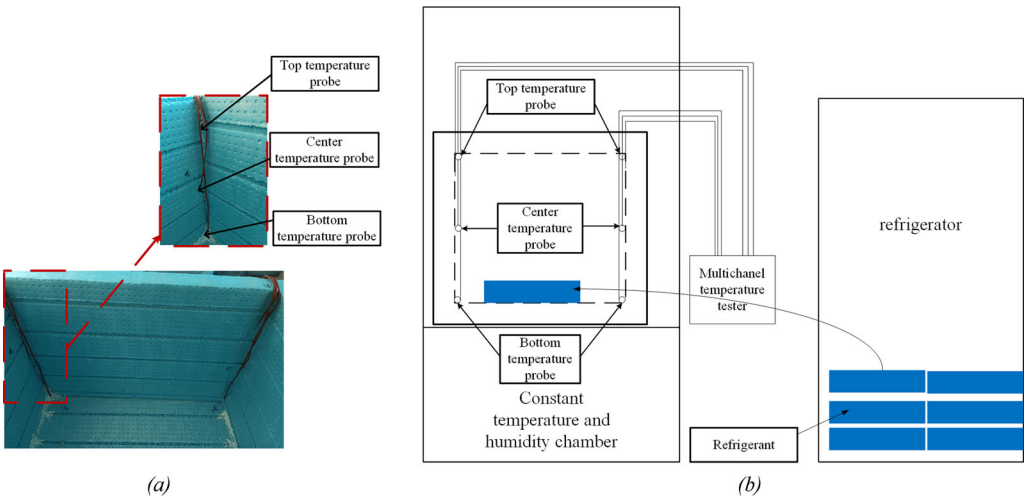

Figure 5. Fixed position of temperature probe in the refrigerator: (*a*) experimental figure and (*b*) schematic of experiment.

350 mm × 250 mm × 250 mm, and wall thickness is 30 mm. The size of the refrigerant is the same as Table 1. The equipment of experiment and their use are shown in Table 4. The accuracy of the multichannel temperature tester is 0.1 °C.

2.3.2. Experimental method

2.3.2.1. Pretreatment..

1. The XPS cold box is placed in a constant temperature and humidity box at the set ambient temperature for 24 h. The refrigerant is placed in a refrigerator at −25 °C for 24 h.
2. The probes of the multichannel temperature tester are fixed on the four inner rings of the bottom, central, and top parts of the box, which is shown in Figure 5.

2.3.2.2. Experimental steps.

1. Twelve probes of the multichannel temperature tester are fixed in the box. Four probes are placed in the refrigerant and then in the constant temperature (25 °C) and humidity box (50%) for 24 h. A total of 24 refrigerants with a side length of 25 mm are placed in a −25 °C refrigerator, pretreated for 24 h, and frozen.
2. The multichannel temperature tester is connected, and the data are recorded.
3. The constant temperature and humidity box is opened, and the temperature and humidity are at 25 °C and 50%, respectively. The pretreated refrigerant is placed in the refrigerator, and a preservative film and tape are used to seal the refrigerator. The sealed refrigerator is then placed in the constant temperature and humidity box.

Table 5. Error between theory and simulation storage times.

Ambient temperature (°C)	Refrigerant (piece)	Storage time (min)		Error (%)
		Theory	Simulation	
25	24	221.7	233	4.38
	48	444.53	456	2.38
	72	667.1	632	5.36
	96	889.67	870	2.30
35	24	158.27	166	4.11
	48	317.48	317	0.30
	72	476.46	460	3.66
	96	635.45	647	1.74
45	24	123.03	123	0.67
	48	246.89	237	4.35
	72	370.55	345	8.45
	96	494.21	486	1.74

Table 6. Error between theory and experiment storage times.

Ambient temperature (°C)	Refrigerant (piece)	Storage time (min)		Error (%)
		Theory	Experiment	
25	24	221.7	234	4.79
	48	444.53	432	30.4
	72	667.1	670	0.36
	96	889.67	854	4.22
35	24	158.27	156	2.04
	48	317.48	314	1.26
	72	476.46	456	4.57
	96	635.45	603	5.43
45	24	123.03	116	6.75
	48	246.89	235	5.24
	72	370.55	342	7.51
	96	494.21	473	4.54

4. When the multichannel temperature tester shows that the temperature inside the box is close to the ambient temperature set, the experiment is completed, and the data are exported and processed in the computer.
5. The experiment is repeated according to Steps (1)–(4) by changing the number of the refrigerant as shown in Table 1.
6. After completing the four groups of 25 °C and 50% humidity experiments, the temperature values are changed to 35 °C and 45 °C. Steps (1)–(5) are repeated, and the experiment is continued until the end.

3. Results

3.1. Accuracy of theoretical model by finite element simulation

The storage time of theoretical model is compared with the simulation results, as shown in Table 5.

According to the comparison between the simulation results and the theoretical model in Table 4, the minimum error of storage time is 0.30% and the maximum is 8.45%. The error between the numerical and theoretical results is due to the fact that the effects of convection heat transfer and gravity on heat transfer are considered into the simulation model, while these are not considered into the theoretical model. The time of simulation results is much longer than that of theoretical model. Therefore, the theoretical model has better computational speed than the simulation model.

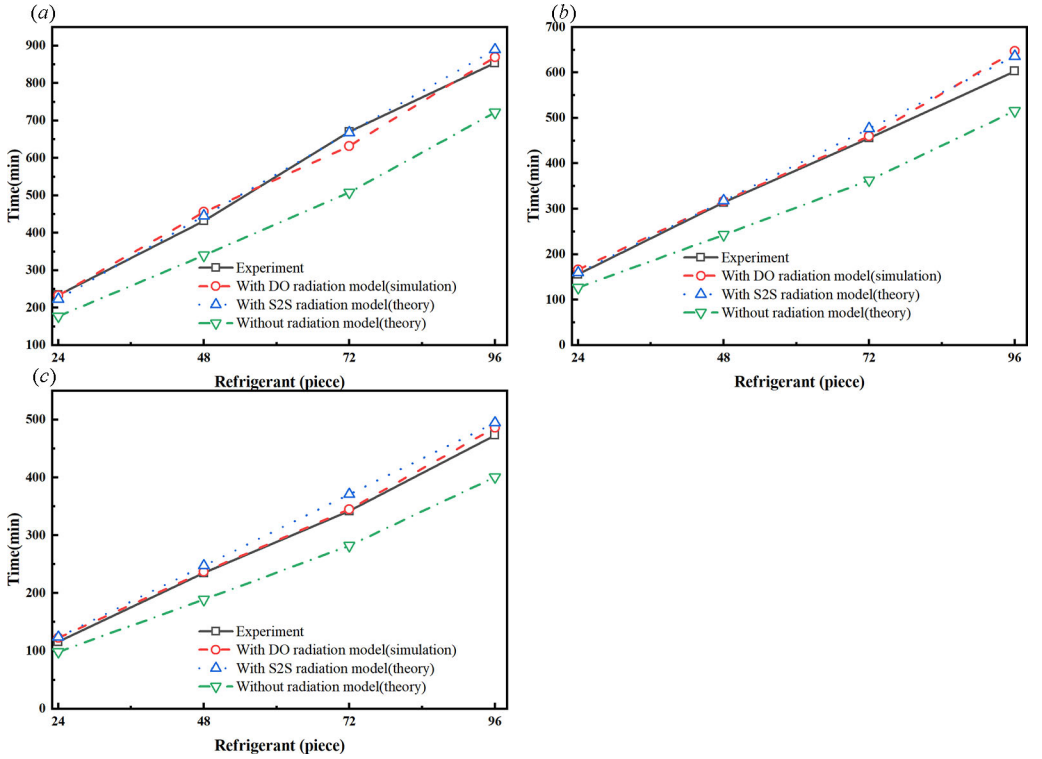

Figure 6. The influence of radiation heat transfer on the storage time of cold box at (*a*) 25 °C, (*b*) 35 °C, and (*c*) 45 °C.

3.2. Accuracy of theoretical model by experiment

The storage time of theoretical modeling is compared with the experimental results, as shown in Table 6.

According to the comparison between the experimental results and the theoretical model calculation in Table 6, the minimum error of storage time is 0.36% and the maximum is 7.51%. The error in experimental and theoretical results is generated by the influence of temperature on the thermal conductivity of materials and the fact that the cold box is not absolutely sealed during the production affect the experimental results.

In conclusion, the storage time calculated by the theoretical model is consistent with experimental thermal storage time.

4. Discussion

4.1. Influence of radiant heat transfer on the cold box

4.1.1. The storage time of cold box

The phase change temperature of ice is 0 °C. Due to the impact of accuracy of the experimental equipment, the storage time of the experiment is the time for the refrigerant to reach 0.1 °C [25]. To analyze the influence of radiation heat transfer on the storage time of cold box, the storage time results with different radiation heat transfer models are compared with experimental results under different amounts of refrigerant and different ambient temperature in Figure 6. The storage time results without radiation heat transfer are vastly different from the experimental results. However, the storage time results with radiation transfer are consistent with experimental results,

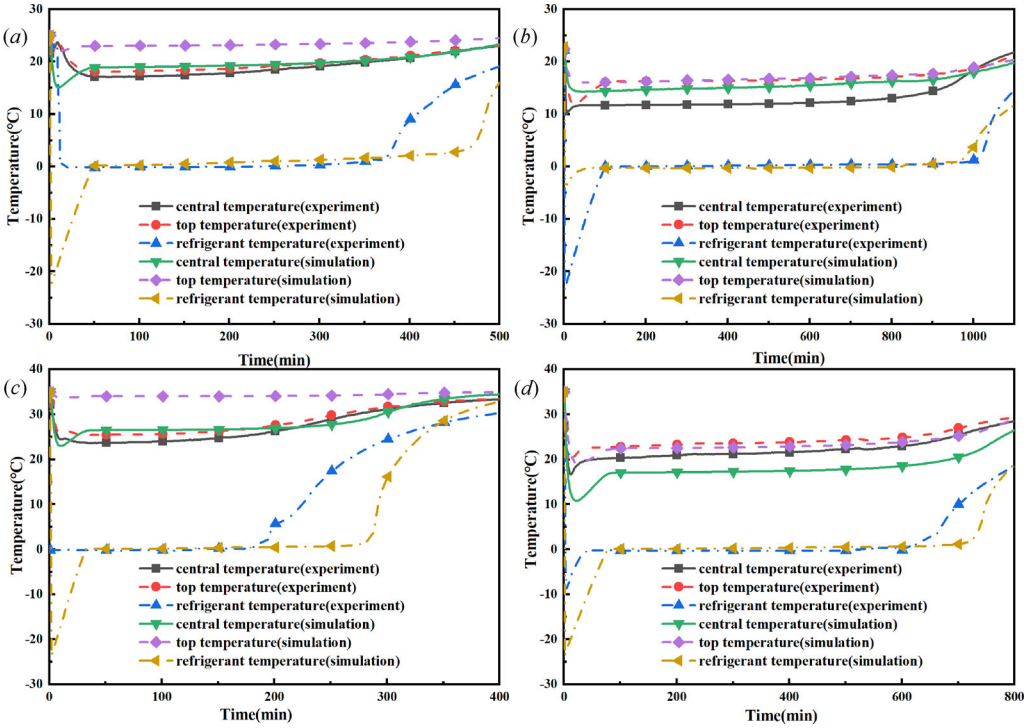

Figure 7. Comparison of the simulation and experimental temperatures: (*a*) 24 refrigerants at 25 °C, (*b*) 96 refrigerants at 25 °C, (*c*) 24 refrigerants at 35 °C, and (*d*) 96 refrigerants at 35 °C.

indicating that the influence of radiation heat transfer on the storage time of the cold box cannot be ignored.

4.1.2. The temperature distribution

Twenty-four and ninety-six refrigerants are used to obtain the simulation temperature results of the refrigerant, the top of cold box, and the center of the cold box at 25 °C and 35 °C. The simulation results are compared with the experimental results, as shown in Figure 7. The middle and top temperatures of the cold box in the simulation results are the same as those in the experimental results, and the coincidence degree between the simulation data and the experimental data is good, indicating that adding the DO radiation model to simulation model can accurately predict the temperature distribution in the cold box.

The simulation results of the refrigerant temperature curve move backward the experimental results, and the simulation shows the super cooling phenomenon [30] because the simulation can more completely present the temperature change from −25 °C to 0 °C. In fact, it takes time for the refrigerant to be taken out from refrigerator and to be placed in the cold box, for the temperature sensor to be attached and for the cold box to be sealed, so the experimental results cannot reach −25 °C and the initial temperature of experimental refrigerant is −5 °C. The temperature results at the top and middle of cold box in the simulation are smaller than the experimental results. It is because that the gaps between the walls of the experimental cold box increase the heat transfer between the environment and the cold box.

Numerical simulation is adopted to conduct a numerical analysis of the temperature changes in the box to analyze the influence of S2S radiation model and the DO radiation model on the temperature of the cold box. The temperature distribution cloud diagrams are obtained, as shown in Figure 8. The temperature field distribution in the cold box when the influence of radiation

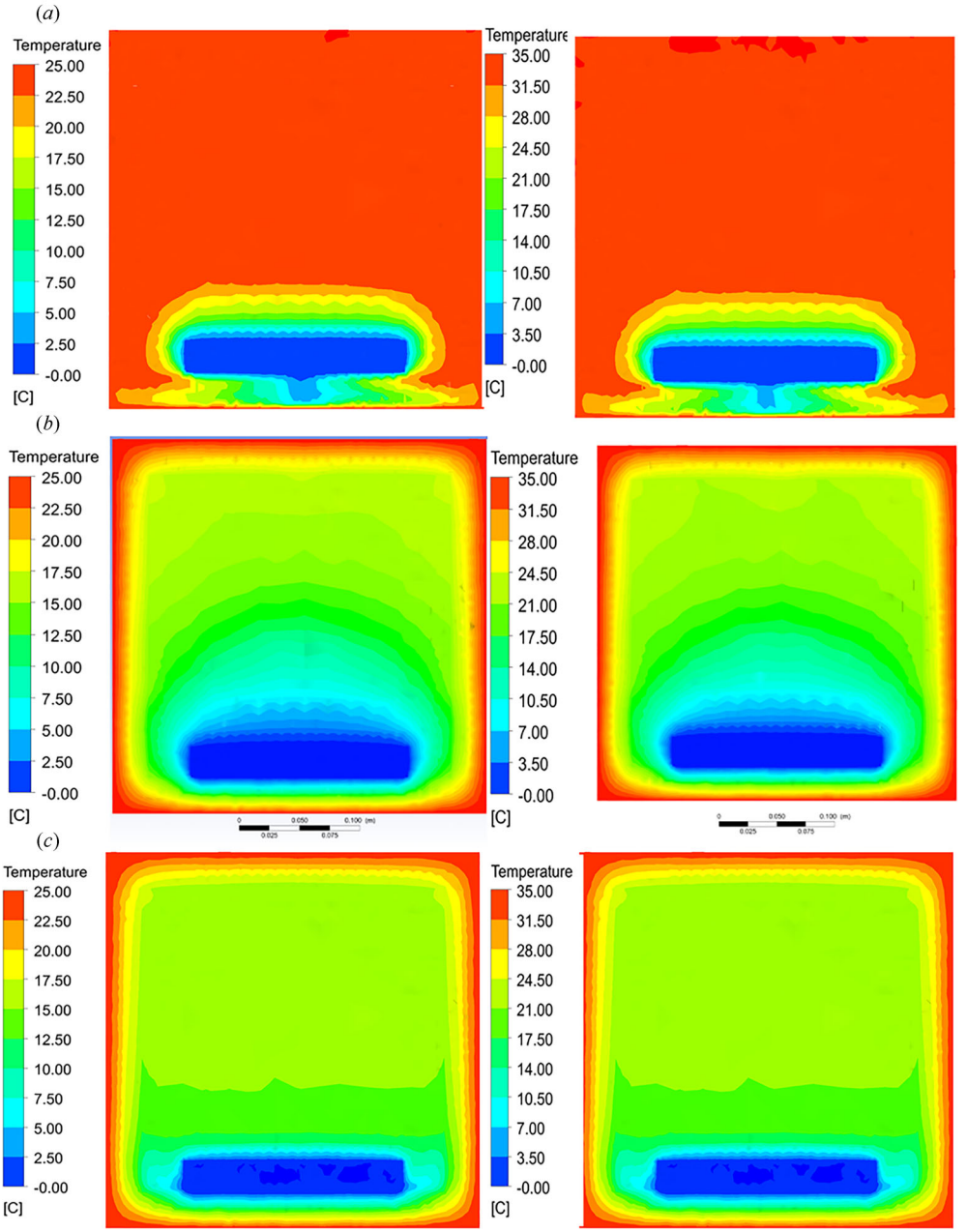

Figure 8. Temperature field cloud chart: (*a*) left is without radiation model with 96 refrigerants at 25 °C, right is without radiation model with 96 refrigerants at 35 °C (*b*) left is with DO radiation model with 96 refrigerants at 25 °C, right is with DO radiation model with 96 refrigerants at 35 °C, and (*c*) left is with S2S radiation model with 96 refrigerants at 25 °C, right is with S2S radiation model with 96 refrigerants at 35 °C.

heat transfer is ignored is shown in Figure 8*a*, and the low temperature in the cold box that gathers at the bottom of the cold box does not appear in Figure 7 at different locations and temperatures. The temperature field distribution adding DO radiation is shown in Figure 8*b*. The temperature field in the cold box exhibits stratification due to the diffusion of radiation heat transfer to the surrounding. Radiation heat transfer cannot be ignored when the refrigerant is placed at the bottom of the cold box. Combined with Figure 7, adding the DO radiation model

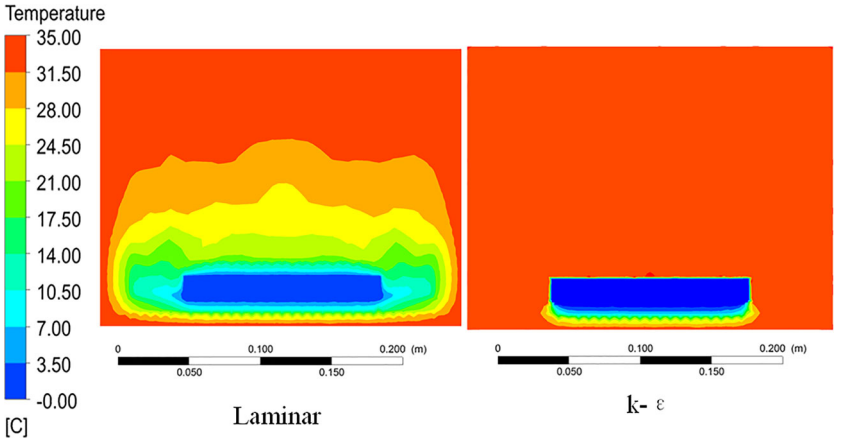

Figure 9. Temperature distribution with different fluid flow models at 35 °C.

to simulation model can accurately predict the temperature distribution in the cold box. The stratification of temperature distribution is not obvious by adding S2Sradiation model, as shown in Figure 8*c*. The temperature difference between the middle and top of the cold box with S2S radiation model is 0.4 °C and the top temperature is lower than center temperature, which are quite different from the experimental results. Therefore, as for the temperature distribution of the cold box, adding the DO radiation model can more accurately distribute than adding S2S radiation model.

In conclusion, the influence of radiation heat transfer on the thermal insulation performance of the cold box cannot be ignored. As for the storage time, adding the S2S radiation model and adding the DO radiation model both can predict well the experimental results. As for the temperature distribution, the DO radiation model can more accurately distribute than the S2S radiation model.

4.2. Influence of convection heat transfer on the cold box

As shown in Figure 8*a*, if the radiation heat transfer were not considered, the temperature distribution in the cold box should be caused by convection heat transfer. To analyze the influence of convection heat transfer on the temperature distribution when the amount of refrigerant is 72 and these are placed at the bottom of the cold box under 35 °C, the fluid flow model is set to laminar and $k - \varepsilon$ models in the simulation. The temperature distribution is shown in Figure 9. The air temperature distribution inside the box is affected by both temperature difference and gravity. The cold air in the box both accumulates at the bottom with different fluid flow models, indicating that convective heat transfer can be neglected when the refrigerant is placed at the bottom.

4.3. Influence of solid sensible heat on theoretical modeling of storage time

Solid sensible heat must be studied with ΔE_{st} when calculating the storage time of the box, as shown in Figure 10. In Figure 10, the theoretical results of the box are significantly lower than the experimental results when no solid sensible heat is added into ΔE_{st}. The calculated results are in good agreement with the experimental results when solid sensible heat is added to the theoretical construction. Therefore, solid sensible heat must be added when constructing a theoretical model of storage time.

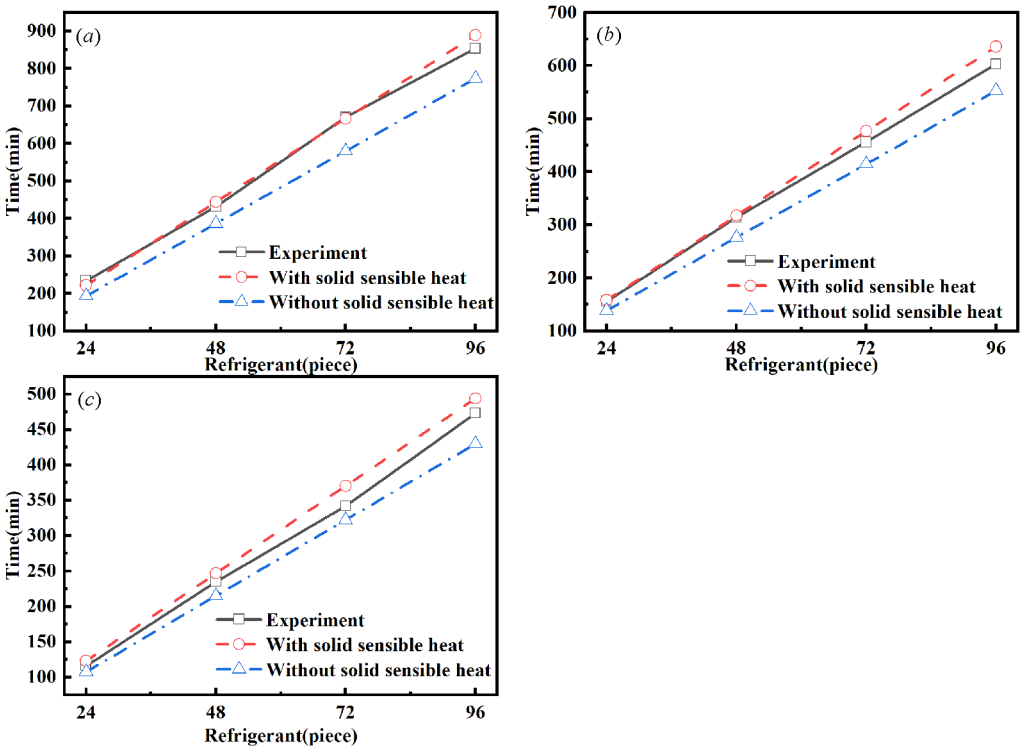

Figure 10. Storage time of the experimental and theoretical models with or without solid sensible heat: (*a*) 25 °C, (*b*) 35 °C, and (*c*) 45 °C.

Table 7. Thermal conductivity and storage time of different materials.

Materials	Thermal conductivity ($W \cdot m^{-1} \cdot °C^{-1}$)	Theoretical modeling (min)	Simulation modeling (min)	Error (%)
VIP [9]	0.004	1114.18	1084	2.78
EPU [9]	0.026	171.41	166	3.26
EPS [31]	0.04	111.42	114	2.26

4.4. Stability of theoretical modeling

Figure 6 shows that the numerical model can also efficiently predict the experimental results. Therefore, the stability of the theoretical model is studied by using a numerical model.

The simulation and theoretical modeling results are compared under different cold box and refrigerant materials to study the stability of the theoretical model.

4.4.1. Different cold box materials

The thermal conductivity of three cold box materials used to verify the theoretical and simulation model is shown in Table 6. Ice is still used as the refrigerant. The initial temperature of refrigerant is −5 °C, while the ambient temperature is 25 °C. The results of storage time calculated by two models are shown in Table 7.

The maximum error between the theoretical and the simulation models is 3.26%, indicating that the theoretical modeling can efficiently predict the storage time under different cold box materials, as shown in Table 7.

Table 8. Thermal physical properties of different refrigerant materials.

Materials	Thermal conductivity ($W \cdot m^{-1} \cdot °C^{-1}$)	Latent heat ($J \cdot g^{-1}$)	Freezing temperature (°C)	Specific heat ($J \cdot kg^{-1} \cdot °C^{-1}$)
H_2O + 1%PAAS [1]	0.7570	335.4	−0.037	2562
H_2O + 1%PAAS + 0.1%MWCNT [1]	0.9021	334.4	−0.294	2311
SP-50 [27]	0.6	190	−55.15	2000

Table 9. Storage time of simulation and theoretical modeling of different refrigerant materials.

Materials	Theoretical modeling (min)	Simulation modeling (min)	Error (%)
H_2O + 1%PAAS [1]	183.83	184	0.09
H_2O + 1%PAAS + 0.1%MWCNT [11]	182.33	183	0.37
SP-50 [27]	81.86	82	0.17

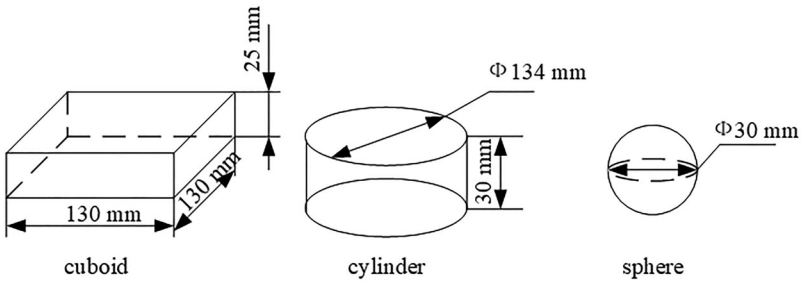

Figure 11. Different shapes of refrigerant.

Table 10. Compared with theoretical model and simulation model under different shapes of refrigerant.

Shape of refrigerant	Theoretical model (min)	Simulation model (min)	Error (%)
Cuboid	222.8	233	4.38
Cylinder	235.6	245	3.84
Sphere	346.8	358	3.13

4.4.2. Different refrigerant materials

The thermophysical property of three refrigerant materials used to verify the theoretical and simulation model is shown in Table 8. The quality of the refrigerant and cold box materials should be the same as before. The temperature between the ambient and phase change of refrigerant is set at 25 °C. The results of storage time calculated by two models are shown in Table 9.

Table 9 illustrates that the maximum error between the theoretical and the simulation model is 0.37%, indicating that the theoretical modeling can efficiently predict the storage time under different refrigerant materials. In conclusion, the storage time of theoretical modeling has stability under the different cold box and refrigerant materials.

4.4.3. Different shapes of refrigerant

To explore the applicability of the theoretical model in different shapes of the refrigerant, the shape of the refrigerant was changed on the basis of keeping the quality of the refrigerant unchanged, as shown in Figure 11. The refrigerant is placed at the bottom of the cold box, the ambient temperature is 25 °C, and the initial temperature of the accumulator is −5 °C. The simulation and theoretical model results, as shown in Table 10. The maximum error is 4.38%, indicating that the theoretical model can be used to calculate the storage time of the different shapes of refrigerant.

5. Conclusion

In this work, the influence of the radiation heat transfer on the cold box and the influence of adding different radiation models on cold box are studied. The results show that the storage time and the temperature distribution are consistent with experimental results by adding the radiation model, indicating that the influence of radiation heat transfer on the cold box cannot be ignored. The following conclusions can be obtained:

1. As for the storage time, adding the S2S radiation model and adding the DO radiation model both can predict well the experimental results. As for the temperature distribution, the DO radiation model can more accurately distribute than the S2S radiation model.
2. The network method of radiation heat transfer and heat conduction shape factor are used to construct the theoretical model of storage time. The theoretical models with and without sensible heats are compared with the experimental results, indicating that the theoretical model with sensible heat can better predict the experimental results.
3. The theoretical model is compared with the simulation model and experimental results based on the sensible heat and radiation heat transfer. The maximum error between the theoretical and experimental model results is 8.45%, and that between the simulation model and theoretical model results is 7.51%, indicating that the theoretical model can effectively predict the experimental and simulation results.
4. The stability of the theoretical modeling is studied by simulation of different cold box and refrigerant materials, and different shapes of refrigerant. The results show that the maximum error between the simulation and the theoretical results is 4.38% under different box and refrigerant materials, indicating that the theoretical model has stability.

In this work, the network method of radiation heat transfer is calculated, and the sensible heat, shape factor, and radiation heat transfer are used to establish the storage time model of the cold box, which provides a method for calculating the heat transfer in a 3D closed environment. The influence of production in the cold box on storage time will be analyzed in the future.

Declarations

Ethics approval and consent to participate. This work was not applicable for this section.

Consent for publication

All authors approved the final manuscript and the submission to this journal.

Competing interests

All authors certify that they have no affiliations with or involvement in any organization or entity with any financial interest or non-financial interest in the subject matter or materials discussed in this manuscript.

Authors' contributions

Zhiqiang Fu: Conceptualization, methodology, Writing – review & editing, Visualization, Supervision. Haozhe Liu: Conceptualization, methodology, Software, Validation, Data curation, Formal analysis, Investigation, Writing – original draft, Writing – review & editing, Visualization. Liying Duan: Investigation, Visualization. Liqiang Huang: Writing – review & editing, Supervision. Yan Wang: Software, Supervision. All authors have reviewed this manuscript.

Acknowledgment

This work was thanks to Tianjin University of Science and Technology Packaging Innovation Laboratory for providing experimental equipment and site support.

Funding

This work was supported by Tianjin Municipal Education Commission (Grant numbers NO. 2019KJ209).

ORCID

Zhiqiang Fu http://orcid.org/0000-0003-4198-4539
Haozhe Liu http://orcid.org/0000-0003-3162-9883

Availability of data and materials

The datasets generated during and analyzed during the current study are not publicly available, but are available from the corresponding author on reasonable request.

References

[1] X. Xu, X. Zhang, and S. Liu, "Experimental study on cold storage box with nanocomposite phase change material and vacuum insulation panel," *Int. J. Energy Res.*, vol. 42, no. 14, pp. 4429–4438, 2018. DOI: 10.1002/er.4187.

[2] A. Ashok, M. Brison, and Y. Letallec, "Improving cold chain systems: Challenges and solutions," *Vaccine*, vol. 35, no. 17, pp. 2217–2223, 2017. DOI: 10.1016/j.vaccine.2016.08.045.

[3] X. Zhang, "Modelling of the thermal conductivity in cold chain logistics based on micro-PCMs," *IJHT*, vol. 36, no. 3, pp. 1075–1080, 2018. DOI: 10.18280/ijht.360339.

[4] Y. Zhao, X. Zhang, X. Xu, and S. Zhang, "Development of composite phase change cold storage material and its application in vaccine cold storage equipment," *J. Energy Storage*, vol. 30, no. 2020, pp. 101455–101466, 2020. DOI: 10.1016/j.est.2020.101455.

[5] Y. Song et al., "Experimental and numerical investigation on dodecane/expanded graphite shape-stabilized phase change material for cold energy storage," *Energy*, vol. 189, no. 2019, pp. 116175–116182, 2019. DOI: 10.1016/j.energy.2019.116175.

[6] B. Bai, K. Zhao, and X. Li, "Application research of nano-storage materials in cold chain logistics of e-commerce fresh agricultural products," *Res. Phys.*, vol. 13, no. 2019, pp. 102049–102056, 2019. DOI: 10.1016/j.rinp.2019.01.083.

[7] P. Jia, W. Wu, and Y. Wang, "Preparation of 0 °C phase change material and its cold storage performance in cold-chain logistics," *Chem. Ind. Eng. Prog.*, vol. 38, no. 6, pp. 2862–2869, 2019. DOI: 10.16085/j.issn.1000-6613.2018-1611.

[8] M. Ryms and W. M. Lewandowski, "Evaluating the influence of radiative heat flux on convective heat transfer from a vertical plate in air using an improved heating plate," *Int. J. Heat Mass Transf.*, vol. 173, pp. 121232–121247, 2021. DOI: 10.1016/j.ijheatmasstransfer.2021.121232.

[9] J. Du *et al.*, "Cooling performance of a thermal energy storage-based portable box for cold chain applications," *J. Energy Storage*, vol. 28, no. 2020, pp. 101238–101247, 2020. DOI: 10.1016/j.est.2020.101238.

[10] J. Zhao *et al.*, "Recyclable low-temperature phase change microcapsules for cold storage," *J. Colloid Interface Sci.*, vol. 564, no. 2020, pp. 286–295, 2020. DOI: 10.1016/j.jcis.2019.12.037.

[11] D. Wang *et al.*, "Investigation on the storage effect and nutritional quality of peach in cold storage containers transportation with different insulation materials," *Food Sci. Technol.*, vol. 43, no. 2, pp. 58–63, 2018. DOI: 10.13684/j.cnki.spkj.2018.02.011.

[12] T. Wu *et al.*, "Preparation of a low-temperature nanofluid phase change material: $MgCl_2$–H_2O eutectic salt solution system with multi-walled carbon nanotubes (MWCNTs)," *Int. J. Refrig.*, vol. 113, no. 2020, pp. 136–144, 2020. DOI: 10.1016/j.ijrefrig.2020.02.008.

[13] H. Tan, N. Wen, and Z. Ding, "Numerical study on heat and mass transfer characteristics in a randomly packed air cooling tower for large-scale air separation systems," *Int. J. Heat Mass Transf.*, vol. 178, no. 2021, pp. 121556–121567, 2021. DOI: 10.1016/j.ijheatmasstransfer.2021.121556.

[14] X. Xiaofeng and Z. Xuelai, "Simulation and experimental investigation of a multi-temperature insulation box with phase change materials for cold storage," *J. Food Eng.*, vol. 292, no. 2021, pp. 110286–110294, 2021. DOI: 10.1016/j.jfoodeng.2020.110286.

[15] A. Sharma, M. Trivedi, K. Agarwal, and N. Nirmalkar, "Thermal energy storage in a confined cylindrical heat source filled with phase change materials," *Int. J. Heat Mass Transf.*, vol. 178, no. 2021, pp. 121603–121616, 2021. DOI: 10.1016/j.ijheatmasstransfer.2021.121603.

[16] J.-C. Paquette, S. Mercier, B. Marcos, and S. Morasse, "Modeling the thermal performance of a multilayer box for the transportation of perishable food," *Food Bioprod. Process.*, vol. 105, no. 2017, pp. 77–85, 2017. DOI: 10.1016/j.fbp.2017.06.002.

[17] M. A. Khan *et al.*, "Experimentally-Benchmarked kinetic simulations of heat transfer through rarefied gas with constant heat flux at the boundary," *Int. J. Heat Mass Transf.*, vol. 176, pp. 121378, 2021. DOI: 10.1016/j.ijheatmasstransfer.2021.121378.

[18] H. Shen *et al.*, "3D numerical investigation of the heat and flow transfer through cold protective clothing based on CFD," *Int. J. Heat Mass Transf.*, vol. 175, pp. 121305, 2021. DOI: 10.1016/j.ijheatmasstransfer.2021.121305.

[19] F. P. Incropera, D. P. Dewitt, T. L. Bergman, and A. S. Lavine, *Fundamentals of Heat and Mass Transfer*, 6th ed. New York: Wiley, 2014.

[20] A. Ambaw *et al.*, "The use of CFD to characterize and design post-harvest storage facilities: Past, present and future," *Comput. Electron. Agric.*, vol. 93, no. 2013, pp. 184–194, 2013. DOI: 10.1016/j.compag.2012.05.009.

[21] L. Zhang *et al.*, "Wall thickness of incubator at ambient temperature and material thermal conductivity," *Packag. Eng.*, vol. 41, no. 5, pp. 97–102, 2020. DOI: 10.19554/j.cnki.1001-3563.2020.05.013.

[22] H. Zhao *et al.*, "Temperature field simulation method of XPS incubator based on Fluent," *Packag. Eng.*, vol. 39, no. 19, pp. 105–109, 2018. DOI: 10.19554/j.cnki.1001-3563.2018.19.019.

[23] V. K. Mishra and S. Chaudhuri, "Implementation of stochastic optimization method-assisted radial basis neural network for transport phenomenon in non-newtonian third-grade fluids: Assessment of five optimization tools," *Arab. J. Sci. Eng.*, vol. 46, no. 12, pp. 11797–11818, 2021. DOI: 10.1007/s13369-021-05702-8.

[24] K. Anand, A. Bhardwaj, S. Chaudhuri, and V. K. Mishra, "Self-organizing map network for the decision making in combined mode conduction-radiation heat transfer in porous medium," *Arab. J. Sci. Eng.*, vol. 47, no. 12, pp. 15175–15194, 2022. DOI: 10.1007/s13369-021-06489-4.

[25] F. Yu, Y. Li, and Y. Zhu, "Numerical and experimental investigation on the thermal insulation performance of low temperature cold box," *Int. Commun. Heat Mass Transf.*, vol. 36, no. 9, pp. 908–911, 2009. DOI: 10.1016/j.icheatmasstransfer.2009.05.008.

[26] J. Wu and L. Zhang, "Modeling and simulation of an insulated box based on COMSOL and temperature field analysis," *Bull. Sci. Technol.*, vol. 34, no. 08, pp. 84–89 + 94, 2018. DOI: 10.13774/j.cnki.kjtb.2018.08.016.

[27] A. K. Ray, S. Singh, D. Rakshit, and Udayraj, "Comparative study of cooling performance for portable cold storage box using phase change medium," *Therm. Sci. Eng. Prog.*, vol. 27, pp. 101146, 2022. DOI: 10.1016/j.tsep.2021.101146.

[28] M. Krishnani and D. N. Basu, "On the validity of Boussinesq approximation in transient simulation of single-phase natural circulation loops," *Int. J. Therm. Sci.*, vol. 105, pp. 224–232, 2016. DOI: 10.1016/j.ijthermalsci.2016.03.004.

[29] W. Jiang, Q. Liu, and J. Qu, "Study on thermal conductivity of thermal insulation materials under natural climate simulation," *Green Environ. Prot. Build. Mater.*, vol. 09, pp. 1–2, 2020. DOI: 10.16767/j.cnki.10-1213/tu.2020.09.001.

[30] J. Vadhera, A. Sura, G. Nandan, and G. Dwivedi, "Study of phase change materials and its domestic application," *Mater. Today: Proc.*, vol. 5, no. 2, pp. 3411–3417, 2018. DOI: 10.1016/j.matpr.2017.11.586.

[31] X. Pan, D. Wang, and H. Zhu, "Study on temperature field of different materials in incubator," *Food Mach.*, vol. 34, no. 8, pp. 115–118, 2018. DOI: 10.13652/j.issn.1003-5788.2018.08.023.